The International Journal of Advanced Manufacturing Technology (2019) 103:2347–2361
https://doi.org/10.1007/s00170-019-03541-4

ORIGINAL ARTICLE

Design and evaluation of 3D printed polymeric cellular materials for dynamic energy absorption

Fatah Habib[1] · Pio Iovenitti[1] · Syed Masood[1] · Mostafa Nikzad[1] · Dong Ruan[1]

Received: 12 December 2018 / Accepted: 4 March 2019 / Published online: 18 April 2019
© Springer-Verlag London Ltd., part of Springer Nature 2019

Abstract

The design freedom to create complex shapes and parts is one of the major benefits offered by the 3D printing manufacturing process. The aim of this study is to utilize this advantage to tailor and optimize cellular materials for impact energy-absorbing applications. The energy-absorbing performance of two types of lattice structure, namely, octagonal and Kelvin lattices, is investigated numerically and compared to the out-of-plane performance of the traditional honeycomb, under two different loading conditions. Firstly, the relative density of the three structures is kept constant and each structure is subjected to three different compression loading rates. Secondly, the three structures are designed to have the same stress threshold of 1 MPa at a loading rate of 3.5 m/s produced at the maximum energy-absorbing efficiency strain $\left(\varepsilon_{\eta_{\max}}\right)$, and they are subjected to an impact mass and an initial velocity of 1.75 kg and 3.5 m/s, respectively. For the second condition, an empirical relationship is established to relate the design parameters of each structure to the peak stress produced at the $\varepsilon_{\eta_{\max}}$. Compression experiments are performed on the standard specimens of the thermoplastic base material at different strain rates to characterize its dynamic properties and rate sensitivity, for the numerical modeling. The finite element approach is validated against experimental results of published studies. The numerical results show that when the relative density is kept constant, the out-of-plane energy absorption of the traditional honeycomb, which is known for its high-energy absorption, significantly outperforms the two lattices for all loading rates. However, when the stress threshold is kept constant, the results show that both lattices can provide better energy-absorbing performance than the honeycomb. Finally, a methodology is developed to improve the energy absorption of the octagonal lattice and the traditional honeycomb; this enhances their energy-absorbing efficiency significantly, from 57 to 63% and from 44 to 61%, respectively.

Keywords Cellular materials · 3D printing · Graded structures · Johnson-Cook material model · Finite element analysis · Energy absorption

1 Introduction

Mitigating the kinetic energy produced by impact loading is a major design consideration in many engineering applications. These include but are not limited to human protective devices, packaging, and applications in the defense industry. For an energy absorber to be able to protect an object from an impact, it should be able to absorb the dynamic energy produced by the impact without transmitting a stress magnitude higher than the maximum permitted stress level (threshold) to the protected object [1–3].

The unique compressive behavior of cellular materials, including their high specific strength, large densification strain, and potential for a smooth and consistent stress plateau through the long strain stroke, makes them an attractive solution for energy-absorbing applications. In addition, cellular materials offer a range of design variables for optimizing energy absorption, including topology and microstructure, cell size, and cell wall material [4].

The design freedom offered by 3D printing can turn virtually any tailored design of a cellular structure, regardless of its complexity, into reality. This allows freedom in designing, manipulating, and optimizing the micro-architecture of a cellular material to achieve the desired mechanical and energy-absorbing characteristics.

✉ Fatah Habib
fhabib@swin.edu.au

[1] Department of Mechanical and Product Design Engineering, Faculty of Science, Engineering and Technology, Swinburne University of Technology, Melbourne 3122, Australia

Due to the complexity and vast expense of experimental investigations, researchers [5–12] have used the finite element method (FEM) to study the structural and energy-absorbing properties of cellular materials. It has been demonstrated that the FEM is a cost-effective and efficient engineering tool to analyze and predict the quasi-static and dynamic energy-absorbing and mechanical behavior of cellular materials with good accuracy if used properly.

Studying the energy-absorbing behavior of materials and structures usually starts with quasi-static analysis and testing. This is more convenient to perform, and quasi-static characteristics include the predominant geometrical effects, which also occur under dynamic loading [1]. The quasi-static energy-absorbing behavior of cellular materials has been extensively studied. For instance, Fan et al. [13] studied the energy-absorbing mechanism of tubular structures and proposed higher-order tubular lattice structures to enhance the energy-absorbing efficiency. Habib et al. [5–7] studied quasi-static energy-absorbing behavior and efficiency of polymeric honeycombs and lattice structures of different cell geometries fabricated by different 3D printing techniques. Michailidis et al. [14] experimentally studied the compressive properties and energy absorption characteristic of aluminum alloy foams manufactured by a powder metallurgy technology. Al-Saedi et al. [15] studied the compressive properties and energy-absorbing capability of functionally graded aluminum alloy lattice fabricated by selective laser melting (SLM). The quasi-static study can give a useful understanding of the energy-absorbing behavior of a material or structure with less effort and cost; however, it may not represent the most real-life energy-absorbing applications that occur under dynamic loading.

The dynamic energy-absorbing mechanism of a cellular material is more complicated than the quasi-static one. That is due to two factors, which do not exist in the quasi-static condition. Firstly, the flow stress of most materials under high strain rates does not remain the same as in the quasi-static case. Thus, the rate dependency of the material should be considered. Secondly, in dynamic events, the mode of deformation for an energy absorber might be totally different from that in the quasi-static condition due to inertia effects, which are produced when regions of the structure experience high acceleration during an impact [16].

Researchers have studied dynamic energy absorption of cellular materials. Shen et al. [17] experimentally investigated the compressive and energy-absorbing behavior of closed-cell aluminum foams at high strain rates. Xu et al. [18] studied the out-of-plane dynamic compressive response and energy absorption of hexagonal honeycombs. Chen et al. [19] numerically studied the dynamic behavior and energy absorption of closed-cell metal foams of functionally graded densities. Rajendran et al. [20] used a drop hammer to perform experimental tests to investigate impact-absorbing characteristics of a closed cell aluminum foam. In another study [21], they examined the effect of filling stainless tubes with a closed cell aluminum foam on improving the energy-absorbing performance of the combination compared to using the foam and the stainless tubes separately. Harris et al. [4] investigated the impact response of stainless steel hybrid lattice materials fabricated via selective laser melting (SLM) process. It was demonstrated experimentally how an additive manufacturing route could be exploited to add geometric complexity to the material microstructure, creating a robust basis for geometry optimization. Cui et al. [22] proposed a functionally graded foam, in which the density was varied throughout the thickness of the foam block, to improve the impact absorption properties of uniform foam. The published literature creates a good foundation in this field. However, there is a need to demonstrate how an energy absorber can be designed for a specific impact protection application and what the criteria are, and why a certain structure is preferred over the others, and how its energy-absorbing performance can be optimized. Answering these questions is the scope of this study.

In this work, compression experiments were performed on standard specimens of the thermoplastic base material (PA12) at different strain rates to characterize its dynamic response and rate sensitivity for the finite element (FE) simulations. The dynamic energy-absorbing behavior of two types of PA12 lattice structures, namely, octagonal and Kelvin lattices [7], was studied by means of FE simulation under different dynamic loading conditions. A systematic approach was used to assess the energy-absorbing capacity of these lattices and compared with the out-of-plane performance of a well-known high energy-absorbing structure, namely, the hexagonal honeycomb, and the best structure for each loading condition was identified. Finally, an optimization methodology was proposed to enhance the energy-absorbing performance of the octagonal lattice and the traditional honeycomb.

2 Structures' design

Two types of regular lattice structures, namely, octagonal and tetrakaidecahedral (Kelvin) lattices [7], and a traditional hexagonal honeycomb were designed. Each lattice was constructed by building unit cells of $5 \times 5 \times 5$ mm^3 in size and duplicating them in three dimensions to make a lattice structure of $5 \times 6 \times 6$ cells in height, width, and depth, respectively. The honeycomb was prismatic in height with 7×6 cells in width and depth, respectively, and was constructed from uniform hexagonal cells of 5 mm in cell size. Since the relative density (RD) is the most important feature of cellular materials [2], the three structures were designed to have an identical relative density of 15%.

All cell struts of each lattice were a cylinder of uniform length l and diameter d throughout the structure. The cell walls

of the hexagonal honeycomb had an identical length and thickness of *l* and *t*, respectively. The CAD models of the three structures and detailed design parameters of a unit cell and the overall specimen of the three structures are presented in Fig. 1.

A brand of polyamide (PA12) thermoplastic material available for multi-jet fusion (MJF) 3D printing process was considered as the base material for the cellular structures. PA12 is from the nylon family of thermoplastic polymers known for its high toughness and energy-absorbing capability. MJF process was chosen as the additive manufacturing process due to its durability, dimensional accuracy, and capability to make dense and nearly isotropic parts more rapidly than the traditional 3D printing systems [7, 23].

3 Material characterization

In order to simulate and reliably predict the structures' response to the quasi-static and dynamic loadings, the behavior of the base material (PA12) under large strains and various strain rates needed to be characterized.

The raw material of PA12 thermoplastic provided by HP Inc., in a powder form was used along with the HP fusing agent on the HP Jet Fusion 4200 3D system to produce standard compression test specimens. The MTS Criterion Electromechanical Universal Test System (Model 43) with 50-kN load cell was used for the low strain rate compression tests, and the Split Hopkinson's Pressure Bar (SHPB) was used for the high strain rate compression tests at room temperature. To ensure the repeatability of the experimental tests, at least three samples were tested for each test condition.

Standard cylindrical specimens of 12.7 mm in diameter and 50.8 mm in length with the loading rate of 1.3 mm/min were used to determine the elastic modulus and offset yield stress, as recommended by ASTM D695–15 [24]. It was assumed that the elastic behavior of the material is rate-insensitive and remains constant for all strain rates.

The post-yield nominal stress-strain data at low strain rates were obtained from the compression tests performed at strain

Cellular structure designation	Unit cell design and parameters			CAD model of cellular specimens		
	CAD model	*l*	*d or t*	Top view	Isometric view	Dimensions
Octagonal lattice	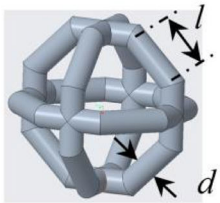	2.071	*d* = 0.813	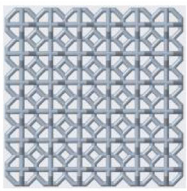	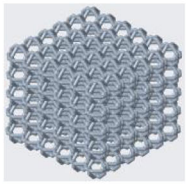	Height = 25 + *d* Width = 30 + *d* Depth = 30 + *d*
Kelvin lattice	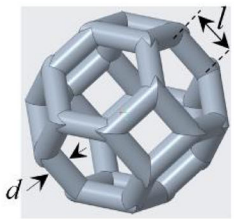	1.768	*d* = 0.748	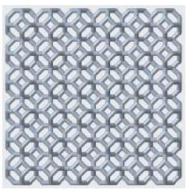		Height = 25 + *d* Width = 30 + *d* Depth = 30 + *d*
Hexagonal honeycomb	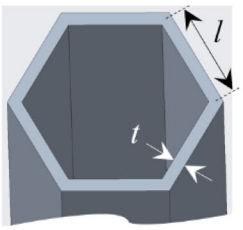	2.887	*t* = 0.362	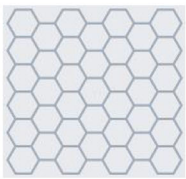	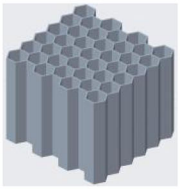	Height (out-of-plane) = 25 Width = 31.76 + *t* Depth = 30 + *t*

Fig. 1 Unit cell and overall specimen design and dimensions for the examined 3D structures of 15% relative density (units are in mm)

Table 1 Material properties of PA12 determined from the compression tests and used in the FEM

Elastic modulus	Poisson's ratio[a]	Density[a]	0.2% offset yield stress	Strain rate sensitivity, C
1300 MPa	0.33	919 kg/m^3	36 MPa	0.05

[a] From [7]

rates of 2×10^{-3}, 2×10^{-2}, 2×10^{-1}, and 5×10^{-1} s^{-1} on the standard test specimens used for strength measurements (cylindrical specimens of 12.7 mm diameter and 25.4 mm in length), as recommended by the ASTM D695-15 standard.

SHPB was used to perform compression tests at a high strain rate of 3×10^3 s^{-1}. The diameter of the striker, incident, and transmission bars was 14.5 mm. The dynamic compression samples used on SHPB were of cylindrical shapes of 11 mm in diameter and 6 mm in length [25, 26].

The resulting post-yield nominal stress-strain data from the low and high strain rate tests were converted to the true stress-strain data using Eqs. (1) and (2).

$$\sigma_{\text{true}} = \sigma_{\text{nominal}}(1-\varepsilon_{\text{nominal}}) \quad (1)$$

$$\varepsilon_{\text{true}} = \ln(1-\varepsilon_{\text{nominal}}) \quad (2)$$

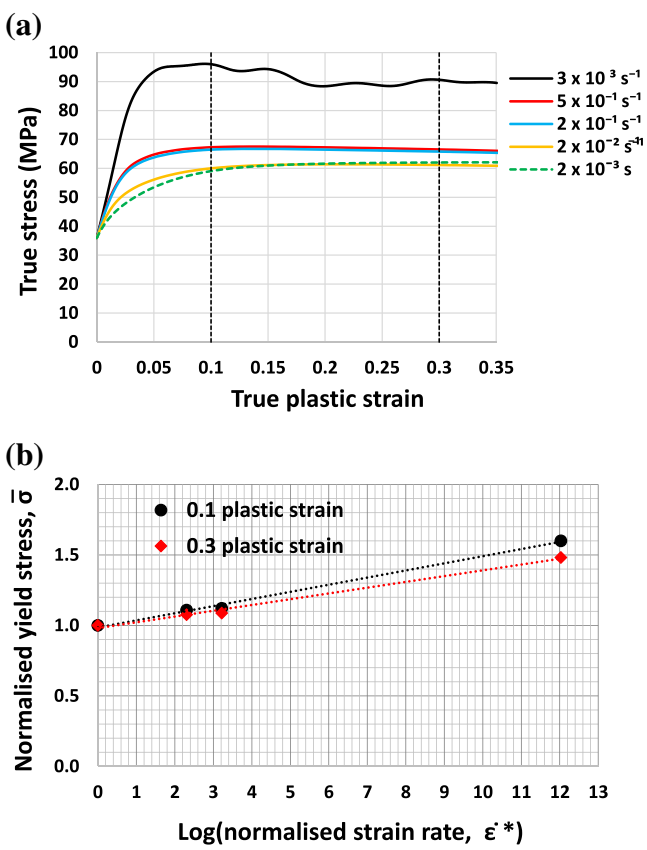

Fig. 2 **a** True stress vs. true plastic strain curves achieved for PA12 at different strain rates and **b** normalized yield stress $\overline{\sigma}$ plotted as a function of log $\dot{\varepsilon}^*$, normalized strain rate, at 0.1 and 0.3 plastic strains

Typical true stress vs. true plastic strain curves generated from each set of compression tests at various strain rates are presented in Fig. 2a. Each curve is a representative of a set of at least three repeated test results. It can be observed that the PA12 material is moderately sensitive to the applied strain rate, as the flow stress increases moderately with the strain rate. At the extremely high strain rate of 3×10^3 s^{-1}, fluctuations of stress are observed.

In this study, the Johnson-Cook (J-C) plasticity model was used to model the hardening behavior and the strain rate dependency of PA12 material. The J-C material model [27, 28] is widely used to capture the strain rate sensitivity of materials. Although this material model was originally developed for metals, it has been shown that it can capture the loading behavior of thermoplastics well, but it is unable to capture the unloading cycle due to the viscoplastic nature of these materials [29].

Since the time interval of the dynamic impacts in this study is considerably small (i.e., the viscoplasticity effect can be ignored), the material acts like a rigid ductile polymer and the unloading cycle is not of interest; therefore, the use of J-C material model is justified.

In the J-C model the yield stress is given by the following Eq. (3) [27, 28]:

$$\sigma = \left[A + B\varepsilon_p{}^n\right]\left[1 + Cln\left(\dot{\varepsilon}^*\right)\right]\left[1-T^{*m}\right] \quad (3)$$

where A, B, n, C, and m are the model constants that need to be determined from experimental tests; ε_p is the accumulated plastic strain; $\dot{\varepsilon}^* = \dot{\varepsilon}_p/\dot{\varepsilon}$ is a dimensionless strain rate; $\dot{\varepsilon}$ is the reference strain rate; and T^* is the temperature variation effect.

As the sensitivity of the material to the variation in temperature is not of interest in this study, Eq. (3) can be reduced to

$$\sigma = \left[A + B\varepsilon_p{}^n\right]\left[1 + Cln\left(\dot{\varepsilon}^*\right)\right] \quad (4)$$

In this reduced equation, A is the yield stress; B and n are the strain-hardening coefficient and exponent, respectively, at the reference strain rate $\dot{\varepsilon}$; and C is the slope of the fitted line for the normalized yield stress $\overline{\sigma}$ plotted as a function of log $(\dot{\varepsilon}^*)$ at a certain plastic strain, where $\overline{\sigma}$ is given by

$$\overline{\sigma} = \frac{\sigma}{\left[A + B\varepsilon_p{}^n\right]} \quad (5)$$

In the present study, the reference strain rate was taken as 2×10^{-2} s^{-1}. In Eq. (5), the term $[A + B\varepsilon_p{}^n]$ is a prediction for the yield stress at a plastic strain ε_p for the reference strain rate $\dot{\varepsilon}$. However, to obtain more accurate results, in this study the yield stress for the reference strain rate $\dot{\varepsilon}$ at each plastic strain was taken from the test data rather than the $[A +$

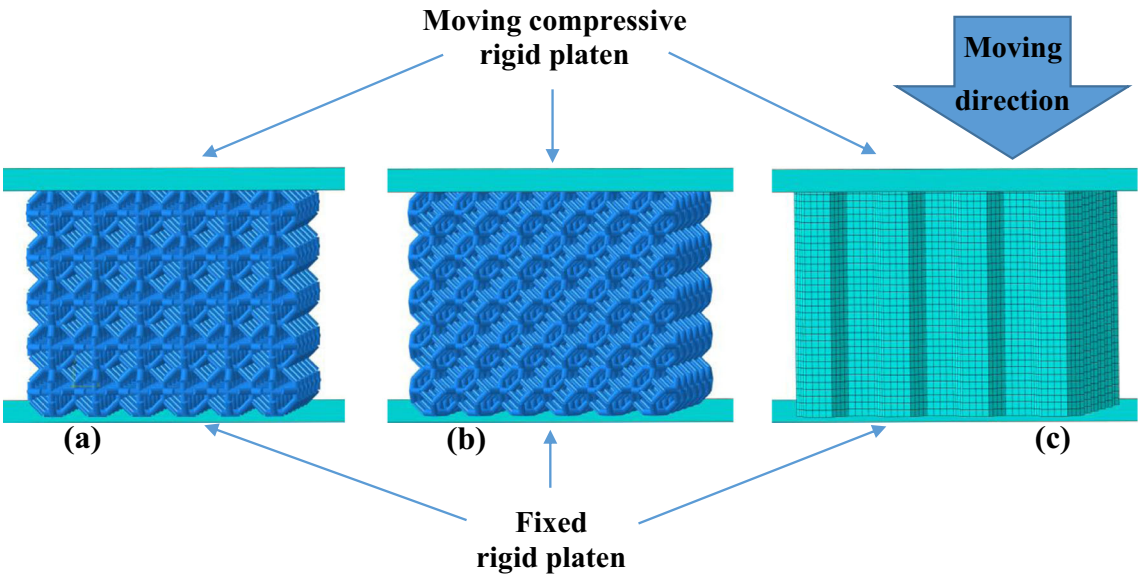

Fig. 3 FE model of simulated structures of 15% relative density under compression **a** octagonal lattice, **b** Kelvin lattice, and **c** hexagonal honeycomb in the out-of-plane direction

$B\varepsilon_p{}^n$] prediction. Figure 2b shows two sets of data for $\overline{\sigma}$ plotted as a function of log $(\dot{\varepsilon}^*)$ at two different plastic strains of 0.1 and 0.3. The slope of the fitted line was calculated for each set of data. The average of the two values was taken as the strain rate sensitivity parameter, C, for the J-C material model. Material properties determined in this section and used in FE simulations in the next sections are listed in Table 1. By comparing compression properties of PA12 presented in Table 1 with tensile properties published in [7, 23] it can be concluded that the MJF PA12 material is slightly stronger in compression than in tension. However, as it can be seen in the Sect. 4.2, that does not make a significant difference in the FEA results.

4 Nonlinear finite element modeling

In this study, the compressive and energy-absorbing behavior of the three structures were investigated using nonlinear finite element (FE) modeling. ABAQUS/Explicit 2018 code was employed for the FE simulations. Beam elements of type B31 were used to discretize the two lattices, and shell elements of type S4R with reduced integration [30] were used to discretize the honeycomb. In the FE model, the upper and lower plates were assumed to be rigid. All degrees of freedom of the lower platen were constrained. Three rotational and two translational degrees of freedom of the upper moving rigid platen were constrained; thus, it could only move in one direction, up or down. The structures' model sat on the fixed lower platen and the upper platen moved downward to compress the cellular structures. An illustration of the FE model used for the three structures is shown in Fig. 3.

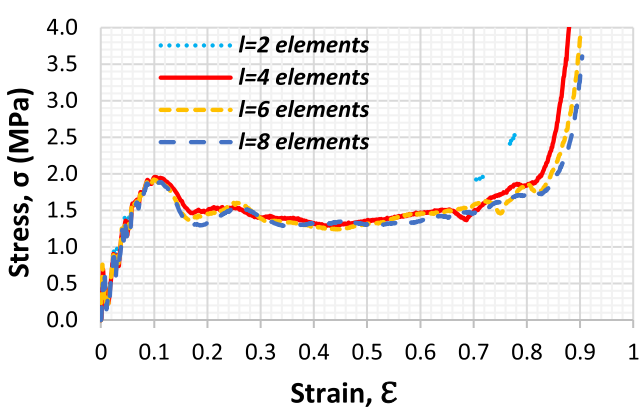

Fig. 4 Stress-strain curves for the octagonal lattice of 15% relative density with various mesh sizes

For the quasi-static compression simulation of such structures, as it is discussed elsewhere [7], it is infeasible to use the standard implicit solver, if not impossible. It is a general practice to use explicit solver for this kind of simulations. When using the explicit solver for quasi-static simulations, there are two methods to achieve an economical solution [31]. The first method involves reducing the time period of the analysis and the second involves using the mass scaling technique. However, the first method is only valid when dealing with the rate-independent base material. Since in this case, the natural time scale is generally not important. In the second method, a limited amount of mass is added to the entire or part of FE model artificially resulting in an increase in the time increment used by ABAQUS/Explicit and a corresponding reduction in computational time. However, it must be ensured that the change in the mass and consequent increase in the inertial forces do not affect the solution significantly.

In this study, for the quasi-static simulations, the first technique was employed, and the velocity of the top rigid compressive platen was artificially increased. The material was assumed to be rate-independent and the true yield stress-true

plastic strain data of the quasi-static material test (2×10^{-3} s^{-1}) was used to define its post-yield behavior. However, for the dynamic loading simulations, the actual time scale and the J-C material model discussed in Sect. 3 with the reference strain stare of 2×10^{-2} s^{-1} and rate sensitivity, C, of 0.05 were used.

4.1 Mesh size sensitivity analysis

A study was conducted on one of the structures (octagonal lattice) to determine the number of beam elements that should be used for the FE modeling of the structures. The aim was to determine the minimal number of elements per edge required to discretize the lattice structure that can produce consistent results with a feasible computational cost. Figure 4 shows the stress-strain curves of the octagonal lattice of 15% relative density at a loading rate of 3.5 m/s when each cell edge of the lattice (l) discretized with two, four, six, and eight elements. It can be seen from Fig. 4 that using four elements per edge can give consistent results with feasible computational cost. In addition, it was observed that using more than four elements per edge may lead to unrealistically increasing the densification strain.

4.2 Validation of the FEA

The FE method described in the previous sections of this study was validated against published experimental works of Habib et al. [7] on PA12 lattices and Xu et al. [18] on aluminum honeycombs. The experimental specimens of the two lattices in [7] were fabricated in PA12 on HP Jet Fusion 4200 3D printer. Three specimens of $5 \times 5 \times 5$ cells from each lattice were tested under the quasi-static compression loading of 5 mm/min [7]. The same specimen size was used in the FE simulations with the material properties determined in Sect. 3. Figure 5a, b compares the quasi-static stress-strain curves obtained from the FE simulations with the experimental curves for the octagonal and Kelvin lattices. Good agreements between the FEA and the experimental results were observed for both lattices. For instance, the percentage of difference between plateau stress [7] calculated from the FEA and experimental results (the average of three samples) for the octagonal and Kelvin lattices was 6.8% and 4.8%, respectively.

The FE method used to simulate the out-of-plane crushing behavior of the honeycomb discussed in the previous sections was validated against a published experimental study by Xu et al. [18] on commercial HexWeb-CRIII aluminum honeycombs. The honeycomb samples used in that study were of 9×9 cells, and the cell wall material was aluminum alloy 5052 with an H39 temper. The input material properties for aluminum 5052 used in the FE validation simulations of the current study were [32] density = 2680 kg/m^3, elastic modulus = 69 GPa, Poisson's ratio = 0.33, yield stress = 292 MPa, and tangent modulus = 690 MPa, and the base material was assumed to be rate insensitive. Figure 5c shows a comparison between our FEA stress-strain curves at two different strain rates of 10^2 s^{-1} and 2×10^2 s^{-1} and Xu et al.'s experimental stress-strain curves. Again, good agreements between the FE method and the experimental results were achieved. The difference between the FEA and experimental plateau stress for the honeycomb [18] at two different strain rates of 10^2 s^{-1} and 2×10^2 s^{-1} was 6.5% and 9%, respectively.

4.3 Energy absorption of structures with the same relative density

To understand the effect of loading rate on the energy-absorbing behavior of the three types of structures, a structure of each type with a constant relative density of 15% was simulated under three constant loading velocities of quasi-static, 3.5 m/s and 35 m/s. The resulting numerical compressive strain vs. transmitted stress to the lower platen (protected side) curves for the three structures are shown in Fig. 6.

The stress-strain curves are analyzed to plot the energy-absorbing efficiency vs. strain curves and to determine the strain corresponding to the maximum energy absorption efficiency $(\varepsilon_{\eta_{\max}})$, which is the optimum limit for using each structure; beyond $\varepsilon_{\eta_{\max}}$, the stress increases rapidly without much increase in absorbed energy. Here the energy absorption efficiency, η, is defined as the ratio of energy absorbed by a cellular material when compressed to a strain ε, to that of the ideal energy absorber (Fig. 7), which transmits the same maximum but constant stress to the protected object when fully compressed throughout its thickness [4, 7, 33], and it is given in Eq. (6):

$$\eta = \frac{\int_0^{\varepsilon} \sigma(\varepsilon) d\varepsilon}{\sigma_p} \tag{6}$$

where $\int_0^{\varepsilon} \sigma(\varepsilon) d\varepsilon$ is the energy absorbed by a cellular structure per unit volume (represented by the area under the stress strain curve) when compressed to the strain ε and σ_p is the maximum stress generated up to the strain ε. These steps are discussed in detail elsewhere [7], and the octagonal stress-stain curve and analysis are illustrated in Fig. 7 as an example.

The energy absorbed by each structure under the three loading conditions up to the strain $\varepsilon_{\eta_{\max}}$ is presented in Fig. 8. The results show that the energy absorption of the three structures increases significantly when the loading rate increases though their produced stress also increases. Also, it can be observed in Fig. 6 and 8 that the compressive strength and energy absorption of the traditional honeycomb is dramatically higher than the two lattice structures. Both the octagonal lattice and the honeycomb generate an initial peak and then soften under the compression, while the Kelvin structure hardens with the increase of strain. In the latter, the stress

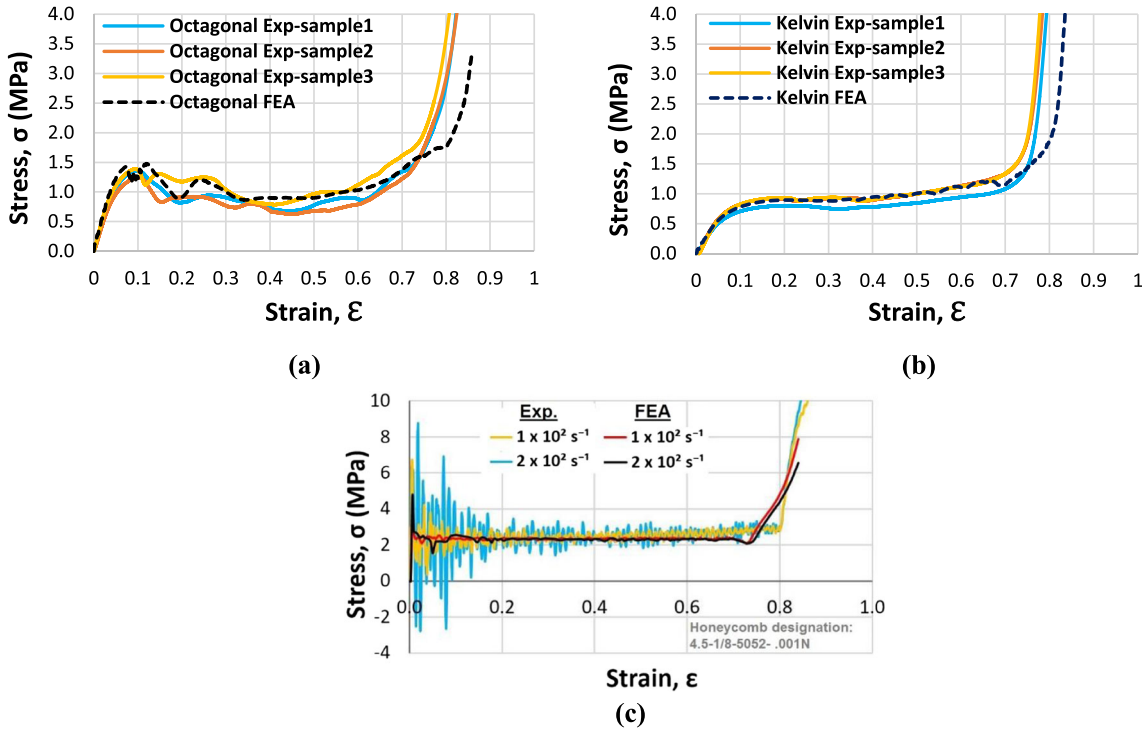

Fig. 5 Validation of the numerical (FEA) method results used in this work against published experimental (Exp) results

seems less sensitive to the loading velocity than the other two structures. This behavior of the Kelvin lattice is in agreement with the remark made by Calladine and English [16].

Another observation that can be made in Fig. 6 for the stress-strain curves at the high loading rate of 35 m/s is that there is a noticeable zero stress region at the

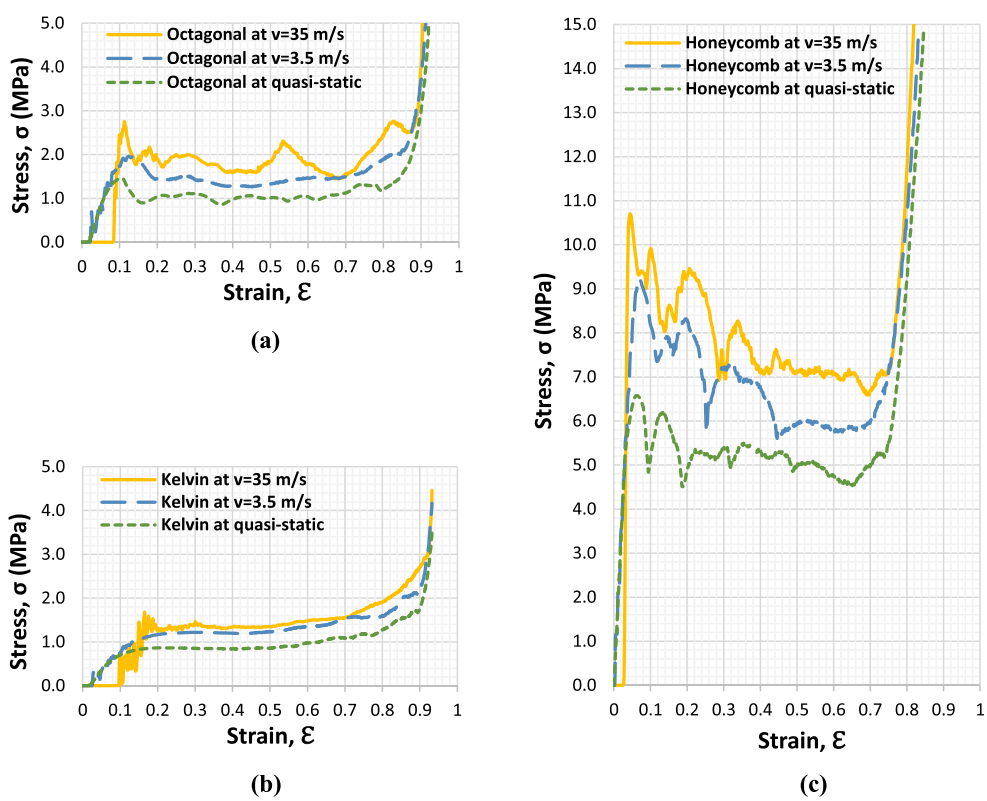

Fig. 6 The numerical stress-strain curves of **a** the octagonal and **b** Kelvin lattices and **c** the traditional honeycomb of constant RD of 15% under different compression loading of quasi-static, 3.5 and 35 m/s

beginning of the loading. This is due to some time delay required to propagate the deformation to the lower platen (protected side).

4.4 Relationship between the design parameters and peak stress

For most applications, such as packaging and human protective devices, there is a stress threshold that the energy absorber must not exceed while absorbing the dynamic impact energy; otherwise, the protected object will be injured (if human) or damaged [1, 2, 6]. In this study, a protective structure to be used as a hip protector was taken as an example. A stress threshold of 1 MPa was taken as the maximum tolerated peak stress, and an initial impact velocity of 3.5 m/s with a mass of 28 kg, as recommended for biomechanical testing of hip protectors [34], was considered for the impact loading. As the specimens used in the present study were smaller than the actual hip protector size by 16 times, the impact mass was scaled down by the same ratio, and a mass of 1.75 kg was considered while the actual impact velocity (3.5 m/s) was kept. Hence, the kinetic energy produced, which is required to be absorbed by a unit volume of the scaled-down energy absorber, was kept constant. Any energy-absorbing structure designed for this application need to be able to absorb the impact energy produced by a mass of 1.75 kg with an impact velocity of 3.5 m/s without exceeding a maximum tolerated stress of 1 MPa. In such simulation, the initial impact velocity (here 3.5 m/s) is required to reach zero at the end of the crushing process of the energy absorber.

Impact simulations were performed on the previous designs of the three structures with RD of 15% (Fig. 1). A mass of 1.75 kg and an initial velocity of 3.5 m/s were assigned to the upper compressive rigid platen. The three structures absorbed the impact energy by deforming until the entire kinetic impact energy had been absorbed, and the velocity of the impact upper platen reached zero. It was observed that the stress-strain curve under the impact loading took nearly the same path of the constant displacement loading of 3.5 m/s until the zero velocity point. At the zero velocity point, the whole impact energy was absorbed and there was no loading on the structure except the weight of the moving upper platen of 1.75 kg. The structures' behavior after this zero point is beyond the scope of this study; it may be able to recover to some extent depending on the base material properties.

As shown in Fig. 9a–c, when the structures are loaded by an impact mass of 1.75 kg with an initial velocity of 3.5 m/s the stress-strain curve takes nearly the same path of the constant displacement loading of 3.5 m/s. The impact energy produced per unit volume of the energy absorbers ($\frac{1}{2}mv^2$ /volume = 0.44 J/cm^3) is absorbed by each structure according to its structural behavior represented by the area under the red curves (Fig. 9).

From Fig. 9a–c, it can be seen that the three structures with the arbitrary relative density of 15% are not suitable for this particular application as they produce higher stress levels than that which can be tolerated. Octagonal lattice, Kelvin lattice and the honeycomb structure produced maximum stresses of 1.9, 1.2, and 9.0 MPa respectively, all exceeding the tolerated stress threshold of 1 MPa. This means that the object (here the human hip bone) cannot be protected by these designs and they may cause a hip fracture if they are used. Figure 9d illustrates the stress-strain behavior of an ideal energy absorber for absorbing the same amount of energy (0.44 J/cm^3) producing the maximum stress of 0.44 MPa, which is much less than the tolerated stress threshold.

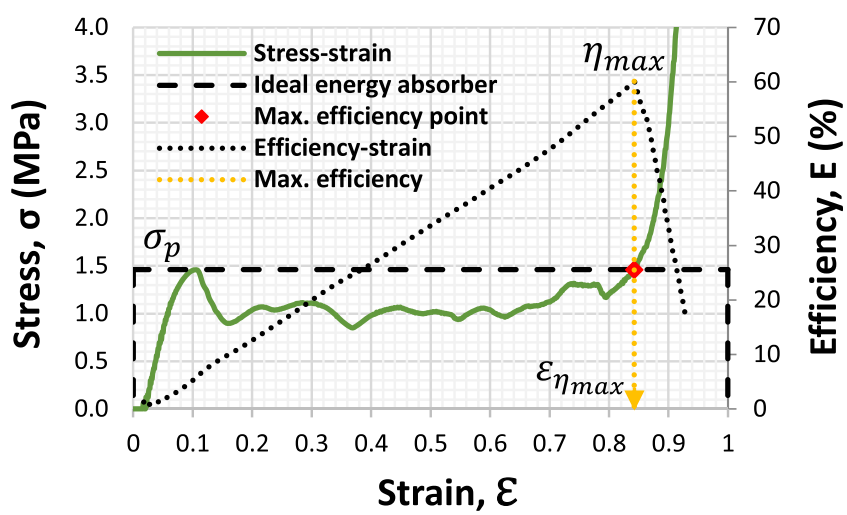

Fig. 7 The stress and energy-absorbing efficiency vs. strain for the octagonal lattice of 15% relative density under quasi-static compression and its corresponding ideal energy absorber which produce the same peak stress, σ_p

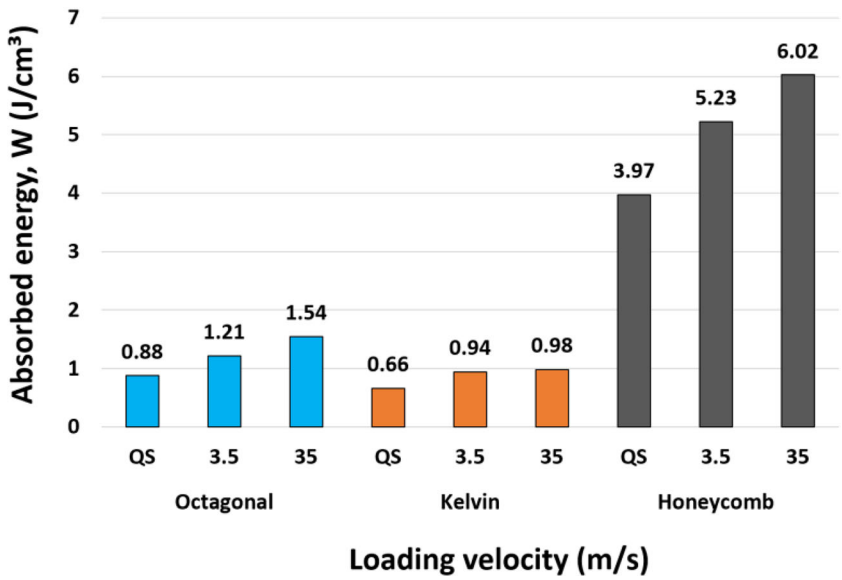

Fig. 8 Energy absorption of the three structures up to the maximum energy-absorbing efficiency strain $(\varepsilon_{\eta_{\max}})$, under three different loading rates of quasi-static (QS), 3.5 m/s and 35 m/s

To design a structure of a required stress threshold for a specific loading velocity, a relationship between the geometric parameters of the structure and the peak stress produced is needed. As the $\varepsilon_{\eta_{\max}}$ (defined in Fig. 7) is the optimum strain limit for using each structure and the stress at the $\varepsilon_{\eta_{\max}}$ is the highest stress up to that limit, the stress at $\varepsilon_{\eta_{\max}}$ is taken as the peak stress and is used in the calculations.

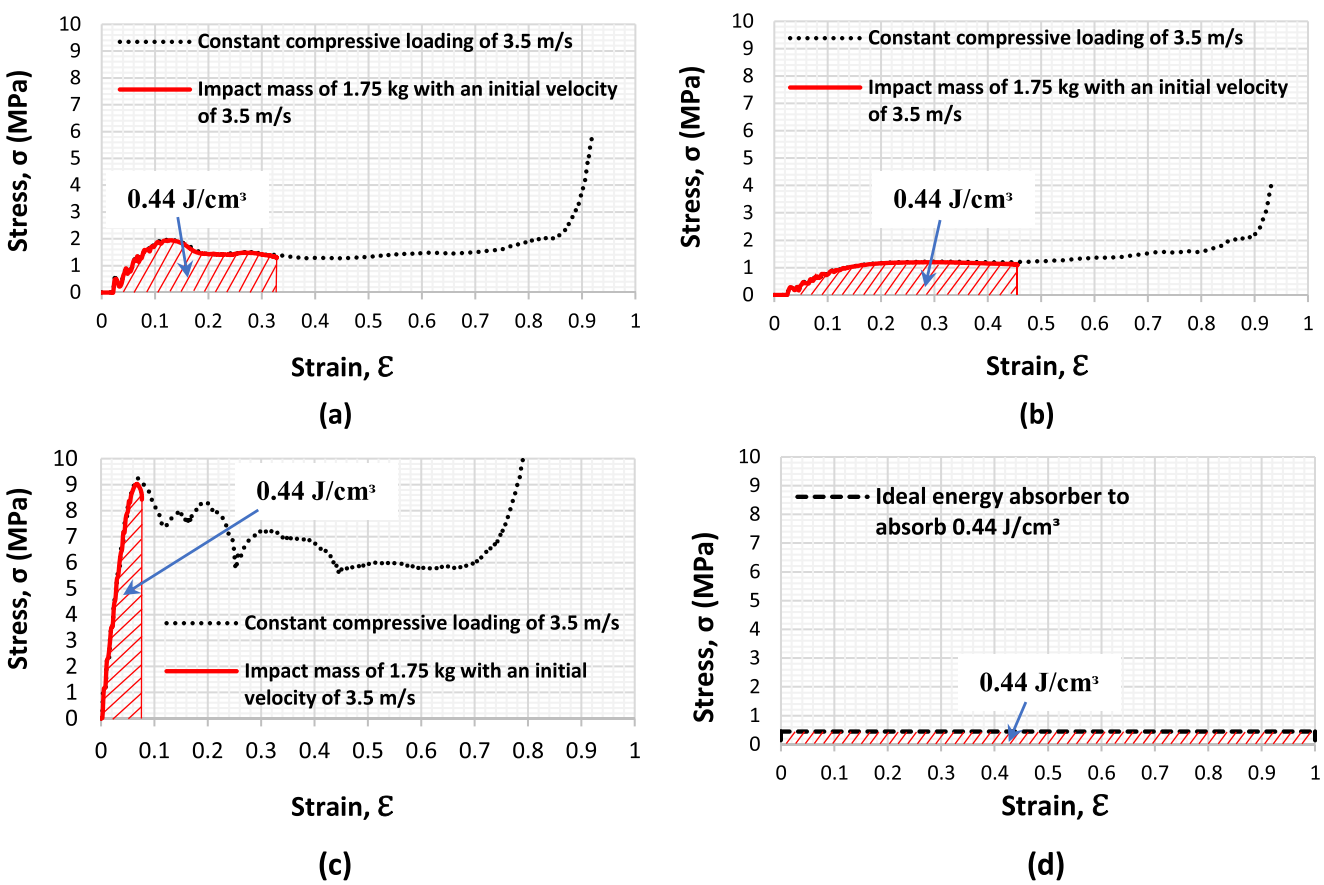

Fig. 9 Stress-strain paths of **a** octagonal and **b** Kelvin lattices, **c** honeycomb structure, and **d** ideal energy absorber, under a constant loading of 3.5 m/s and impact loading of a mass of 1.75 kg with an initial impact velocity of 3.5 m/s

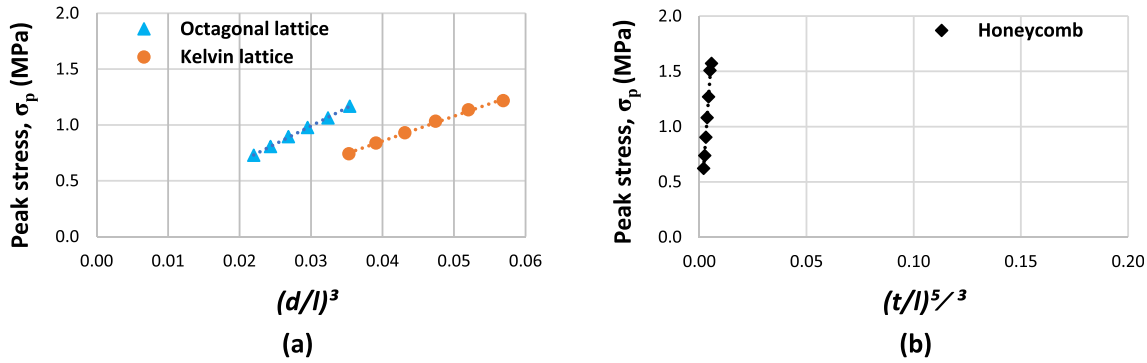

Fig. 10 Peak stress, σp, vs. **a** $(d/l)^3$ of the lattice structures and **b** $(t/l)^{5/3}$ of the honeycomb structure

To establish the relationship between the design parameters and peak stress, six uniform designs with varied (d/l) or (t/l) ratios were created for each of the three types of structures. The unit cell edge length l was kept constant for each structure (illustrated in Fig. 1) and only d or t was varied for each design. Each design was numerically studied under a constant loading velocity of 3.5 m/s. The peak stress produced at the $\varepsilon_{\eta_{max}}$ was determined as discussed in Sect. 4.3 and plotted against their design parameters as shown in Fig. 10a, b. Wierizbicki [2, 35] expressed plastic collapse strength of honeycombs in the out-of-plane direction in terms of $\sigma_y(t/l)^{5/3}$, when σ_y is the yield stress of the base material. The same method was used here to express peak stress, σ_p, of the honeycomb structure. Good agreement with Wierizbicki's equation was observed. For the lattice structures, however, it was observed that the σ_p is linearly related to $(d/l)^3$. The determined relationships are expressed in three empirical equations (Eqs. (7) to (9)). The parameters in the three equations were determined by curve fitting. The three equations imply that the peak stress σ_p increases when the relative density of the cellular structures increases. The high parameter of Eq. (9) indicates the high sensitivity of the honeycomb structure to the relative density, meaning much less dense structure is required for the same stress threshold, σ_p, compared to the octagonal and Kelvin lattices. These equations are used in Sect. 4.5 to design structures with the same stress threshold.

$$\sigma_p \text{ (octagonal lattice)} = 0.918\ \sigma_y\ (d/l)^3 \tag{7}$$

$$\sigma_p \text{ (Kelvin Lattice)} = 0.598\ \sigma_y\ (d/l)^3 \tag{8}$$

$$\sigma_p \text{ (Honeycomb)} = 8.075\ \sigma_y\ (t/l)^{5/3} \tag{9}$$

where σ_y is the yield stress of PA12 and equal to 36 MPa (Table 1).

4.5 Design of structures with the same peak stress

Using the empirical relationships determined in the previous section, a structure of a maximum peak stress of 1 MPa at the maximum efficiency strain $(\varepsilon_{\eta_{max}})$ was designed using the abovementioned Eqs. (7)–(9) for each type. The three structures were simulated under a constant compression loading of 3.5 m/s. The dynamic energy absorption, peak stress, and strain at the $\varepsilon_{\eta_{max}}$ in addition to the design parameters for each structure are listed in Table 2.

It can be seen from Table 2 that all structures have nearly the same intended maximum peak stress of 1 MPa at the $\varepsilon_{\eta_{max}}$. The honeycomb, due to its high compressive strength, has the least relative density (RD) of 4%, but it can absorb only 0.41-J/cm^3 energy up to the stress limit of 1 MPa, meaning that it cannot absorb the required kinetic energy without exceeding the stress threshold (1 MPa). The Kelvin lattice needs the RD of 10.6% to have the same maximum peak stress, and it absorbs 0.56-J/cm^3 energy up to that stress limit. The octagonal lattice with a RD of 9.5% is able to absorb 0.55-J/cm^3 energy

Table 2 Design and energy-absorbing parameters of the examined uniform structures designed to have the same maximum stress threshold of 1 MPa at the $\varepsilon_{\eta_{max}}$ under the loading rate of 3.5 m/s

Cellular structure	Design parameters			Energy absorption parameters at $\varepsilon_{\eta_{max}}$			
	l (mm)	d or t (mm)	RD (%)	$\varepsilon_{\eta_{max}}$	σ_p (MPa)	Energy, W (J/cm^3)	Efficiency, η (%)
Octagonal	2.071	0.64	9.5	0.83	0.97	0.55	57
Kelvin	1.768	0.62	10.6	0.83	0.97	0.56	57
Honeycomb	2.887	0.09	4	0.75	0.94	0.41	44

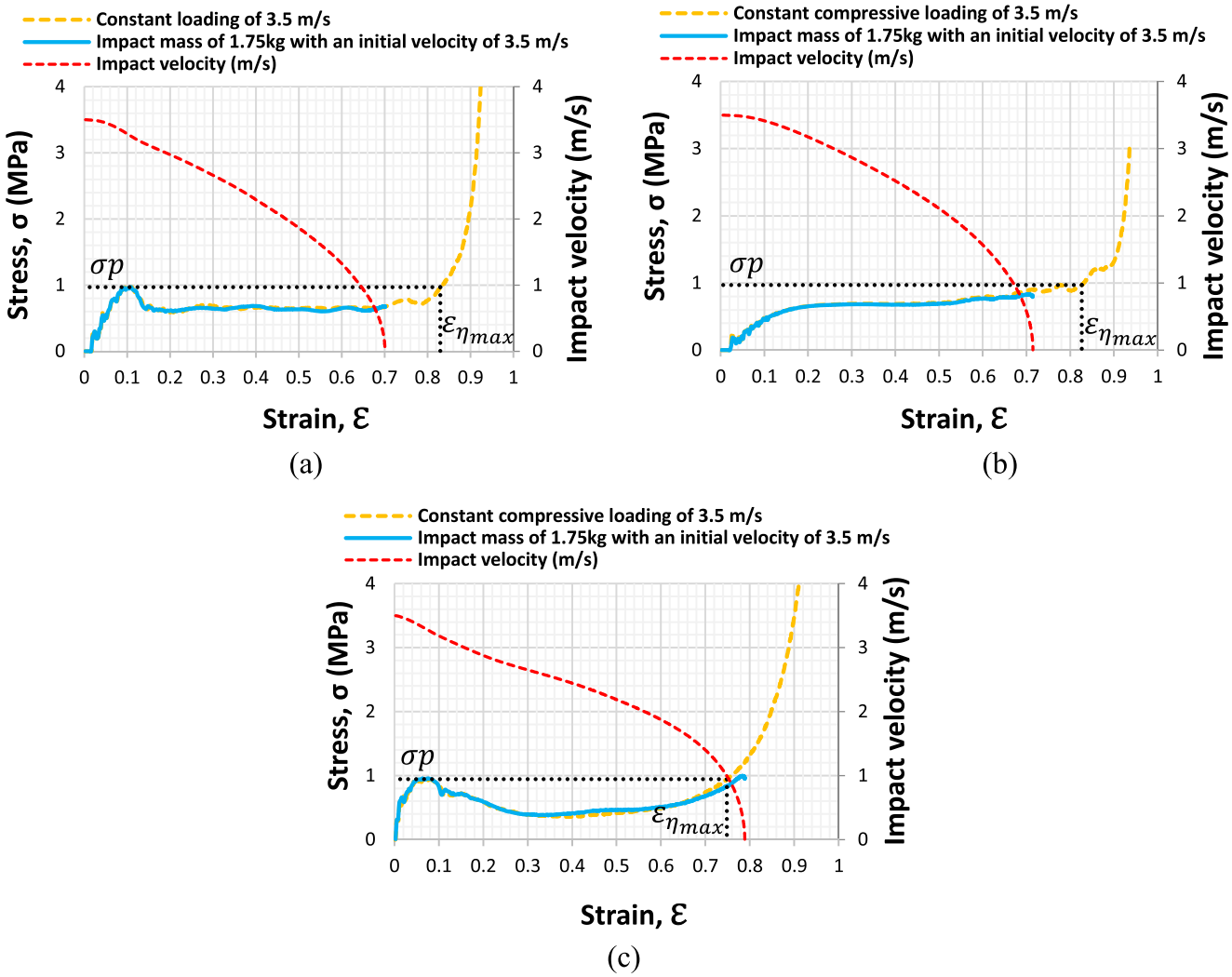

Fig. 11 The stress-strain curves for a constant compressive loading of 3.5 m/s, an impact of 1.75-kg object with an initial velocity of 3.5 m/s combined with the object velocity for the **a** octagonal and **b** Kelvin lattices and **c** the honeycomb of identical σ_p of 1 MPa at $\varepsilon_{\eta_{max}}$

up to the stress limit of 1 MPa. This preliminary analysis shows that, unlike the honeycomb structure, both lattices have potential to absorb the required impact energy of 0.44 J/cm^3 safely within the given stress threshold of 1 MPa.

The impact protection behavior of these structures was simulated under the loading of an impact mass and an initial velocity of 1.75 kg and 3.5 m/s, respectively, as discussed in Sect. 4.4. The stress produced on the protected object (lower plate) and the loading velocity are plotted against the structural strain for the three structures as shown in Fig. 11.

It can be observed from Fig. 11a, b that for both lattice structures the velocity of the impact mass reaches zero (where the blue curve ends) well before their $\varepsilon_{\eta_{max}}$. This indicates that they can absorb 0.44-J/cm^3 impact energy produced by the impact mass effectively and even have potential to absorb some more energy (0.11 J/cm^3 for the octagonal and 0.12 J/cm^3 for the Kelvin) below the stress threshold of 1 MPa. However, for the traditional honeycomb to be able to absorb that amount of energy the stress exceeds the 1 MPa as the structure's deformation exceeds the $\varepsilon_{\eta_{max}}$ limit, as shown in Fig. 11c.

4.6 Enhancing the energy absorption by using density-graded structures

Unlike conventional manufacturing, 3D printing allows tailoring of the cellular structures to obtain the required mechanical behavior. While there is not much that can be done with structures whose stress increases continuously with strain, referred to as type I by Calladine and English [16], such as in Kelvin lattice, it can be hypothesized that the energy-absorbing efficiency of structures that produce the initial peak stress and then soften (type II) can be enhanced using functionally graded designs. Density-graded structures (in the loading direction) allowed by 3D printing can firstly eliminate the initial peak on the stress-strain curve and secondly reduce the

(a)

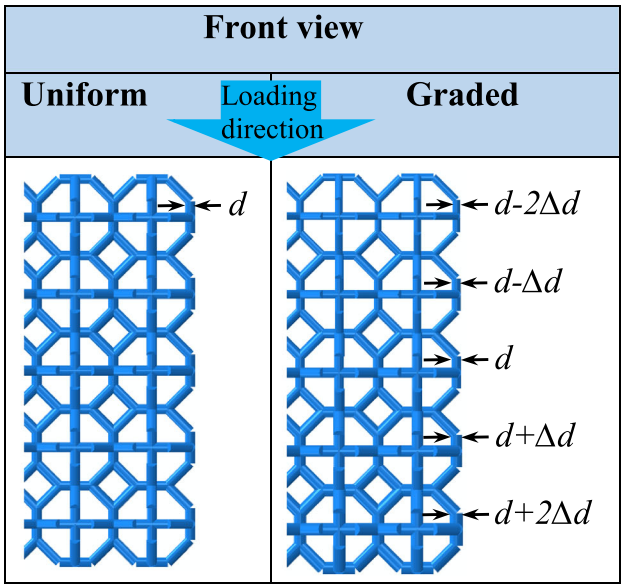

(b)

Design		At the $\varepsilon_{\eta_{max}}$		
Designation	Step, Δd (mm)	W (J/cm$^{3)}$	σ_p (MPa)	η (%)
Uniform	0	0.55	0.97	57
Graded-1	0.08	0.78	2.11	37
Graded-2	0.04	0.63	1.13	56
Graded-3	0.02	0.61	0.99	62
Graded-4	0.01	0.61	0.96	63

Fig. 12 **a** Details of design parameters and **b** energy absorption characteristic for the uniform and four graded octagonal lattices when keeping the cell struts' length and overall structural relative density constant (l = 2.071 mm and d = 0.62 mm)

softening behavior of these structures, thus increasing their energy-absorbing efficiency.

Regular graded structures with different step sizes of Δd and Δt were built from the octagonal lattice and the traditional honeycomb, respectively, as illustrated in Figs. 12 and 14. Cell edge length, l, and the overall relative density for all structures of each type were kept constant and equal to that of the uniform structure, which was discussed in Sect. 4.5. For the graded designs, each row has identical d, or t, but increasing by Δd *or* Δt, respectively, from top to bottom in the loading direction.

Figures 12 and 14 list the design parameters of the uniform and graded structures for the octagonal lattice and the honeycomb, respectively, and their energy-absorbing characteristics obtained from FE simulations under a constant loading velocity of 3.5 m/s. Figures 13a and 15a compare the stress-strain curves of the graded structures to the uniform one for each type of structure. Figures 13b and 15b show the stress-strain and efficiency-strain curves for optimum design of each structure to absorb the maximum energy at the given stress threshold of 1 MPa.

The graded structures allow the plastic deformation to localize initially at the least dense (weakest) row, thus lowering the initial peak stress. Subsequently, the localization propagates through the structure from less to more dense rows, largely eliminating the softening behavior. For the optimum design, this approximates the stress-strain behavior of the structure to that of the ideal energy absorber and increases the energy-absorbing efficiency. By using this methodology, the energy absorption and efficiency of the uniform octagonal lattice were

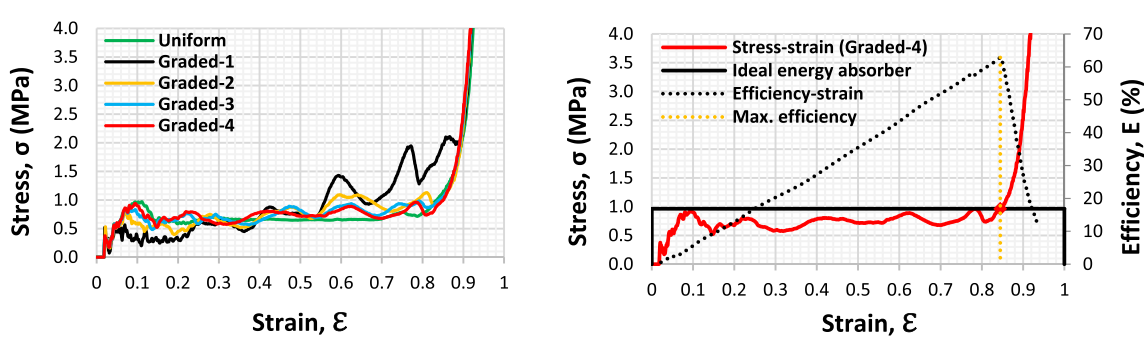

(a) (b)

Fig. 13 **a** Stress-strain curves for uniform and four designs of graded density octagonal lattice structures of identical RD of 9.5%, under constant displacement loading of 3.5 m/s, and **b** stress and efficiency vs. strain for the optimum structure (graded-4) for energy absorption at 3.5-m/s loading rate

(a)

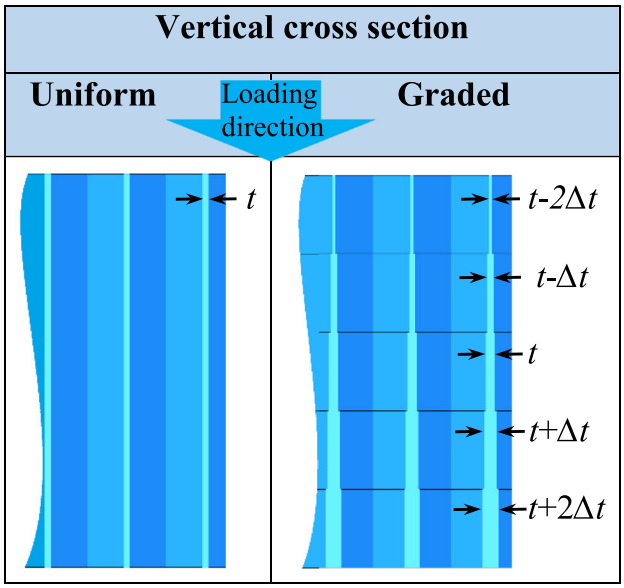

(b)

Design		At the $\varepsilon_{\eta_{max}}$		
Designation	Step, Δt (mm)	W (J/cm^3)	σ_p (MPa)	η (%)
Uniform	0	0.41	0.94	44
Graded-1	0.02	0.72	1.53	47
Graded-2	0.01	0.63	1.06	59
Graded-3	0.005	0.53	0.86	61

Fig. 14 **a** Details of design parameters and **b** energy absorption characteristic for the uniform and three graded hexagonal honeycombs when keeping the cell walls' length and overall structural relative density constant (l = 2.887 mm and t = 0.09 mm)

optimized in the graded design-4 from 0.55 J/cm^3 and 57% to 0.61 J/cm^3 and 63%, respectively, while keeping the stress level below 1 MPa, as shown in Fig. 12. For the honeycomb, these parameters were optimized from 0.41 J/cm^3 and 44% to 0.53 J/cm^3 and 61%, respectively, by graded design-3, whereas the peak produced stress lowered from 0.94 to 0.86 MPa, as listed in Fig. 14.

5 Conclusions

This paper has evaluated energy absorption of two proposed lattice structures, octagonal and Kelvin lattices, and compared their energy-absorbing behavior with a well-known high out-of-plane energy-absorbing structure, namely, hexagonal honeycomb, using FE simulation. The FE method used is validated against published experimental studies. Compression experiments were performed on the standard specimens of the thermoplastic base material (PA12) at different strain rates to characterize its dynamic response and rate sensitivity for the FE simulations. The three structures were initially evaluated at different compression loading rates, with all having the same relative density. The results showed that the traditional honeycomb provided dramatically higher-energy absorption in its out-of-plane direction than the lattices. To compare their energy-absorbing behavior and efficiency for a specific application, a protective structure to act as a hip protector was taken as an example with the stress threshold of 1 MPa and impact mass and initial velocity of 1.75 kg and 3.5 m/s, respectively. An empirical relation was

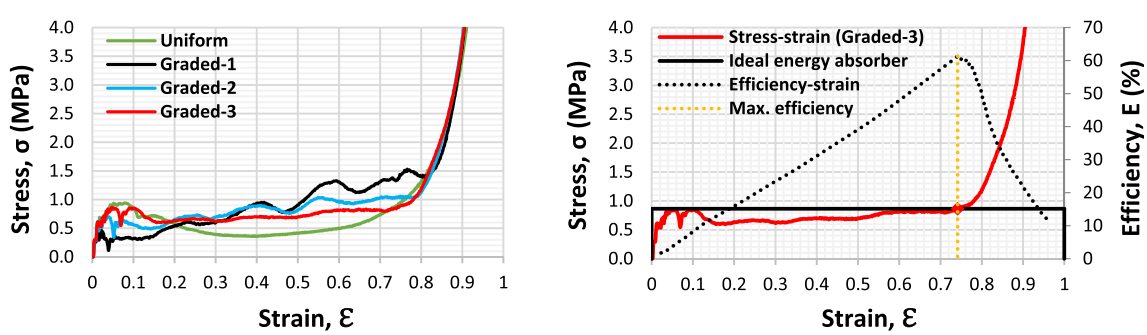

(a) (b)

Fig. 15 **a** Stress-strain curves for uniform and three designs of graded density honeycombs of identical RD of 4% under constant displacement loading of 3.5 m/s and **b** stress and efficiency vs. strain for the optimum structure (graded-3) for energy absorption at 3.5-m/s loading rate

developed between the design parameters and the peak stress produced at the maximum efficiency strain $(\varepsilon_{\eta_{\max}})$, which is the optima for each structure at that loading rate (3.5 m/s). Using these empirical equations, a structure of each type was designed to produce a maximum stress limit of 1 MPa at the $\varepsilon_{\eta_{\max}}$. The performance of these structures was then simulated under an impact loading and velocity of 1.75 kg and of 3.5 m/s, respectively. The numerical results showed that the two lattices were able to absorb the impact energy well before densification. However, in order for the honeycomb structure to be able to absorb that amount of energy, the produced stress exceeded the limit of 1 MPa. Finally, the energy-absorbing behavior of the two strain-softening structures, namely, the octagonal lattice and the honeycomb structure, was enhanced significantly using functionally graded designs. By using density-graded structures the numerical out-of-plane energy absorption of the honeycomb was increased from 0.41 to 0.53 J/cm^3 and efficiency from 44 to 61% while decreasing the maximum produced stress from 0.94 to 0.86 MPa. The graded methodology could improve the numerical energy absorption of the octagonal lattice from 0.55 to 0.61 J/cm^3 and efficiency from 57 to 63% while decreasing the maximum produced stress from 0.97 to 0.96 MPa. This study demonstrates that the process of optimizing the energy absorption of cellular structures has further potential. It was concluded that the energy-absorbing performance and efficiency of 3D printed cellular materials can be improved significantly by using carefully tailored functionally graded structures.

Acknowledgments The authors would like to express their sincere gratitude to Professor Guoxing Lu, Department of Mechanical and Product Design Engineering, Faculty of Science, Engineering and Technology, Swinburne University of Technology, for providing access to ABAQUS software through the Swinburne OzSTAR facility. Dr. Shanqing Xu is acknowledged for his help to conduct the dynamic tests on the material using split Hopkinson pressure bar. The first author appreciates the valuable discussions with Nathan Edwards.

Compliance with ethical standards

Conflict of interest The authors declare that they have no conflict of interest.

References

1. Lu G, Yu T (2003) In: Yu TX (ed) Energy absorption of structures and materials. Woodhead, Cambridge
2. Gibson LJ, Ashby MF (1997) Cellular solids: structure and properties, second edition. Cambridge University Press, Cambridge, pp 1–510
3. Maiti S, Gibson L, Ashby M (1984) Deformation and energy absorption diagrams for cellular solids. Acta Metall 32(11):1963–1975
4. Harris J, Winter R, McShane GJ (2017) Impact response of additively manufactured metallic hybrid lattice materials. Int J Impact Eng 104:177–191
5. Habib FN, Iovenitti P, Masood SH, Nikzad M (2017) In-plane energy absorption evaluation of 3D printed polymeric honeycombs. Virtual Phys Prototyp 12(2):117–131
6. Habib FN, Iovenitti P, Masood SH, Nikzad M (2018) Cell geometry effect on in-plane energy absorption of periodic honeycomb structures. Int J Adv Manuf Technol 94(5–8):2369–2380
7. Habib FN, Iovenitti P, Masood SH, Nikzad M (2018) Fabrication of polymeric lattice structures for optimum energy absorption using multi jet fusion technology. Mater Des 155:86–98
8. Ozdemir Z, Hernandez-Nava E, Tyas A, Warren JA, Fay SD, Goodall R, Todd I, Askes H (2016) Energy absorption in lattice structures in dynamics: experiments. Int J Impact Eng 89:49–61
9. Papka SD, Kyriakides S (1994) In-plane compressive response and crushing of honeycomb. J Mech Phys Solids 42(10):1499–1532
10. Papka SD, Kyriakides S (1998) In-plane crushing of a polycarbonate honeycomb. Int J Solids Struct 35(3):239–267
11. Papka SD, Kyriakides S (1998) Experiments and full-scale numerical simulations of in-plane crushing of a honeycomb. Acta Mater 46(8):2765–2776
12. Alomarah A, Ruan D, Masood S, Sbarski I, Faisal B (2018) An investigation of in-plane tensile properties of re-entrant chiral auxetic structure. Int J Adv Manuf Technol 96(5–8):2013–2029
13. Fan H, Luo Y, Yang F, Li W (2018) Approaching perfect energy absorption through structural hierarchy. Int J Eng Sci 130:12–32
14. Michailidis N, Stergioudi F, Tsouknidas A (2011) Deformation and energy absorption properties of powder-metallurgy produced Al foams. Mater Sci Eng A 528(24):7222–7227
15. Al-Saedi DS, Masood S, Faizan-Ur-Rab M, Alomarah A, Ponnusamy P (2018) Mechanical properties and energy absorption capability of functionally graded F2BCC lattice fabricated by SLM. Mater Des 144:32–44
16. Calladine C, English R (1984) Strain-rate and inertia effects in the collapse of two types of energy-absorbing structure. Int J Mech Sci 26(11–12):689–701
17. Shen J, Lu G, Ruan D (2010) Compressive behaviour of closed-cell aluminium foams at high strain rates. Compos Part B 41(8):678–685
18. Xu S, Beynon JH, Ruan D, Lu G (2012) Experimental study of the out-of-plane dynamic compression of hexagonal honeycombs. Compos Struct 94(8):2326–2336
19. Chen D, Kitipornchai S, Yang J (2018) Dynamic response and energy absorption of functionally graded porous structures. Mater Des 140:473–487
20. Rajendran R, Sai KP, Chandrasekar B, Gokhale A, Basu S (2008) Preliminary investigation of aluminium foam as an energy absorber for nuclear transportation cask. Mater Des 29(9):1732–1739
21. Rajendran R, Sai KP, Chandrasekar B, Gokhale A, Basu S (2009) Impact energy absorption of aluminium foam fitted AISI 304L stainless steel tube. Mater Des 30(5):1777–1784
22. Cui L, Kiernan S, Gilchrist MD (2009) Designing the energy absorption capacity of functionally graded foam materials. Mater Sci Eng A 507(1–2):215–225
23. O'Connor HJ, Dickson AN, Dowling DP (2018) Evaluation of the mechanical performance of polymer parts fabricated using a production scale multi jet fusion printing process. Addit Manuf 22: 381–387
24. ASTM, ASTM D695-15 standard test method for compressive properties of rigid plastics. 2015
25. Kariem M, Ruan D, Beynon J, Prabowo D (2017) Mini round-Robin test on the split Hopkinson pressure bar. J Test Eval 46(2): 1–12
26. Kariem MA, Beynon JH, Ruan D (2012) Misalignment effect in the split Hopkinson pressure bar technique. Int J Impact Eng 47:60–70

27. Johnson GR (1983) A constitutive model and data for metals subjected to large strains, high strain rates and high temperatures. In: Proceedings of the 7th International Symposium on Ballistics, The Hague, Netherlands
28. Banerjee A, Dhar S, Acharyya S, Datta D, Nayak N (2015) Determination of Johnson cook material and failure model constants and numerical modelling of Charpy impact test of armour steel. Mater Sci Eng A 640:200–209
29. Bergstrom JS (2015) Mechanics of solid polymers: theory and computational modeling. William Andrew, USA
30. SIMULIA (2016) Abaqus 6.14 analysis user's guide, Volume IV: Elements. ABAQUS Documentation V6
31. Systemes D (2014) Abaqus 6.14 analysis user's guide, volume II: analysis
32. Xu S, Ruan D, Beynon JH (2014) Finite element analysis of the dynamic behavior of aluminum honeycombs. Int J Comput Methods 11(supp01):1344001
33. Miltz J, Gruenbaum G (1981) Evaluation of cushioning properties of plastic foams from compressive measurements. Polym Eng Sci 21(15):1010–1014
34. Robinovitch SN, Evans SL, Minns J, Laing AC, Kannus P, Cripton PA, Derler S, Birge SJ, Plant D, Cameron ID, Kiel DP, Howland J, Khan K, Lauritzen JB (2009) Hip protectors: recommendations for biomechanical testing-an international consensus statement (part I). Osteoporos Int 20(12):1977–1988
35. Wierzbicki T (1983) Crushing analysis of metal honeycombs. Int J Impact Eng 1(2):157–174

Publisher's note Springer Nature remains neutral with regard to jurisdictional claims in published maps and institutional affiliations.